PHYSICAL REVIEW D **75,** 083006 (2007)

Galactic antiproton spectrum at high energies: Background expectation versus exotic contributions

Torsten Bringmann*
SISSA/ISAS, via Beirut 2-4, 34013 Trieste, Italy

Pierre Salati†
Université de Savoie, 73011 Chambéry, France,
and Laboratoire de Physique Théorique LAPTH, 74941 Annecy-le-Vieux, France
(Received 23 January 2007; published 27 April 2007)

A new generation of upcoming space-based experiments will soon start to probe the spectrum of cosmic-ray antiparticles with an unprecedented accuracy and, in particular, will open up a window to energies much higher than those accessible so far. It is thus timely to carefully investigate the expected antiparticle fluxes at high energies. Here, we perform such an analysis for the case of antiprotons. We consider both standard sources as the collision of other cosmic rays with interstellar matter, as well as exotic contributions from dark matter annihilations in the galactic halo. Up to energies well above 100 GeV, we find that the background flux in antiprotons is almost uniquely determined by the existing low-energy data on various cosmic-ray species; for even higher energies, however, the uncertainties in the parameters of the underlying propagation model eventually become significant. We also show that if the dark matter is composed of particles with masses at the TeV scale, which is naturally expected in extra-dimensional models as well as in certain parameter regions of supersymmetric models, the annihilation flux can become comparable to—or even dominate—the antiproton background at the high energies considered here.

DOI: 10.1103/PhysRevD.75.083006 PACS numbers: 98.70.Sa, 95.35.+d, 96.50.sb

I. INTRODUCTION

Since the pioneering works of Victor Hess almost 100 years ago, we know that the earth is constantly exposed to a bombardment of cosmic rays with presumably galactic origin. Extending up to extremely high energies, they mainly consist of protons (90%) and helium (9%), but also contain sizable contributions of other nuclei and antiparticles. Most of these particles have probably been accelerated in the blast waves of supernova remnants, while others—like antiprotons—are rather produced by the spallation of the interstellar medium by primary cosmic rays.

Measurements of the cosmic-ray antiproton spectrum started in the late 1970s and now extend up to energies around 30 GeV [1–4]. The observations can be extremely well described by adopting a production mechanism as indicated above and then propagating the antiprotons through the galactic halo by means of a simple diffusion model [5]. Remarkably, the parameters of this model are essentially fixed by the spectra of other cosmic-ray species, in particular, the boron over carbon (B/C) ratio [6]. With the satellite-borne PAMELA experiment [7] being in orbit since June 2006 and already taking data, and the planned installation of AMS-02 [8] on the international space station by 2007, the near future will witness very accurate and detailed measurements of the antiproton spectrum, in the case of AMS-02 up to energies of around 1 TeV. It is therefore of great interest to extend previous analyses of the background spectrum to higher energies since this will provide an important test of the underlying diffusion model and thus of our understanding of the propagation of cosmic rays through the galaxy. Having this in mind, the first part of the present work is devoted to a careful discussion of the uncertainties in the expected background spectrum at high energies and, as we shall see, how the already available data help to constrain it considerably.

Not only is a thorough understanding of the cosmic-ray antiproton background an interesting issue in itself, it is also a mandatory prerequisite for any attempt to spot possible exotic contributions. The main reason to expect these is the by now well-established existence of dark matter (DM) which, from the most recent measurements of the cosmic microwave background, contributes about 23% to the total energy content of the universe [9]. While the nature of dark matter is still an open question, weakly interacting massive particles (WIMPs) that arise in many extensions to the standard model of particle physics (SM) are very plausible candidates; thermally produced in the early universe, they automatically acquire the right relic density today [10]. As has first been noticed in [11], the self-annihilation of these particles in the galactic halo could then leave an imprint in the antiproton spectrum. Traditionally, one has mainly focused on a possible contribution at rather low energies since first measurements seemed to indicate an excess of antiprotons below the peak at around 1 GeV [12]. With the improved statistics of

*Electronic address: bringman@sissa.it
†Electronic address: salati@lapp.in2p3.fr

follow-up experiments and a better understanding of the production mechanisms, however, the evidence for such an excess disappeared [13]. In this article, we will therefore rather focus on possible exotic signatures at the high energies that soon will be accessible for the first time. To this end, we will compare the situation for three benchmark models of realistic dark matter candidates with masses in the TeV range; the lightest Kaluza-Klein particle (LKP) in models with universal extra dimension [14,15] and the lightest supersymmetric particle (LSP) in the limit where it is a neutralino with a very high Higgsino [16] or Wino [17] fraction, respectively. For earlier work that explicitly studies the effect of dark matter annihilations on the high-energy antiproton spectrum, see e.g. [18–21].

This article is organized as follows. In Sec. II, we briefly review the two-zone diffusion model that is used to propagate charged particles through the galactic halo; as mentioned before, this model provides an excellent fit to the low-energy data. We then continue in Sec. III with a detailed discussion, both numerically and analytically, of the expected antiproton background for energies up to 10 TeV. Section IV introduces the benchmark dark matter models that then will be used to discuss possible signatures for exotic physics in the antiproton flux and the prospects for their detection. In Sec. V, finally, we give a short summary of our results and present our conclusions.

II. PROPAGATION OF CHARGED PARTICLES THROUGH THE GALAXY

Whatever the mechanism responsible for their production, charged cosmic rays subsequently propagate through the galactic magnetic field and bounce off its irregularities—the Alfvén waves. The resulting particle transport is well described by space diffusion with a coefficient

$$K(E) = K_0 \beta \mathcal{R}^{\delta}, \tag{1}$$

which increases as a power law with the rigidity $\mathcal{R}$ of the particle. In addition, since these scattering centers move with a velocity $V_a \sim 20$ to 100 km s^{-1}, a second order Fermi mechanism is responsible for some diffusive reacceleration. Its coefficient K_{EE} depends on the particle velocity β and total energy E and is related to the space diffusion coefficient $K(E)$ through

$$K_{EE} = \frac{2}{9} V_a^2 \frac{E^2 \beta^4}{K(E)}. \tag{2}$$

In the case of nuclei and antiprotons, one also has to take into account that a certain energy loss rate $b^{\rm loss}(E)$ is induced by adiabatic and Coulomb energy losses, as well as by ionization. Finally, galactic convection wipes cosmic rays away from the disk with a velocity $V_C \sim 5$ to 15 km s^{-1}. After these preliminaries, and equipped with all the necessary notation, we may now write the master equation for the distribution function $\psi = dn/dE$ in space and in energy as

$$\partial_z (V_C \psi) - K \Delta \psi + \partial_E \{ b^{\rm loss}(E) \psi - K_{EE}(E) \partial_E \psi \} = q. \tag{3}$$

This equation applies to any species—protons, antiprotons or positrons—as long as the rates for production q and energy loss $b^{\rm loss}(E)$ are properly accounted for. This general framework—summarized in Eq. (3)—may be implemented within the semianalytical two-zone model which is extensively discussed in [5,6] and whose salient features are briefly recalled here.

In this approach, a steady state is assumed and the diffusive halo is pictured as a thick wheel which matches the circular structure of the Milky Way. The galactic disk of stars and gas—where primary cosmic rays are accelerated—lies in the middle. It extends radially 20 kpc from the center and has a half-thickness h of 100 pc. Confinement layers where cosmic rays are trapped by diffusion lie above and beneath that disk. The intergalactic medium starts at the vertical boundaries $z = \pm L$ as well as beyond a radius of $r = R \equiv 20$ kpc. Notice that the half-thickness L of the diffusive halo is not known and reasonable values range from 1 to 15 kpc. The diffusion coefficient K is the same everywhere while the convective velocity is exclusively vertical with component $V_C(z) = V_C \mathrm{sign}(z)$. The galactic wind—produced by the bulk of the disk stars like the Sun—drifts away from them along the vertical directions, hence the particular form assumed here for V_C. The spallation of the interstellar gas by cosmic rays takes place in the disk. It leads to the production of secondary species like boron or antiprotons. The latter is a background against the neutralino annihilation signal and will be discussed in Sec. III.

The diffusive halo is axisymmetric and the cosmic-ray density vanishes at the radius $R = 20$ kpc. This condition is naturally implemented by the following series expansion for ψ:

$$\psi(r, z, E) = \sum_{i=1}^{+\infty} P_i(z, E) J_0(\alpha_i r/R). \tag{4}$$

The Bessel function of zeroth order J_0 vanishes at the points α_i. The radial dependence of ψ is now taken into account by the set of its Bessel transforms $P_i(z, E)$. The source term q may also be Bessel expanded into the corresponding functions $Q_i(z, E)$ and the master equation (3) thus becomes

$$\partial_z (V_C P_i) - K \partial_z^2 P_i + K \left\{ \frac{\alpha_i^2}{R^2} \right\} P_i + 2h\delta(z) \partial_E \{ b^{\rm loss}(E) P_i - K_{EE}(E) \partial_E P_i \} = Q_i(z, E). \tag{5}$$

Here, energy loss and diffusive reacceleration are confined inside the galactic disk—which is considered infinitely

thin, hence the presence of an effective term $2h\delta(z)$. The form of the source term $Q_i(z, E)$ that appears in Eq. (5) depends on the type of the particle species that is considered. In the case of antiprotons, the following mechanisms can in principle contribute:

(i) Antiprotons may collide elastically on interstellar H and He. Because they are preferentially scattered forward, however, such interactions are innocuous and will be disregarded.

(ii) Antiprotons may also annihilate on interstellar H and He. This leads to a negative source term $-\Gamma_{\bar{\mathrm{p}}}^{\mathrm{ann}}\psi$, where the annihilation rate $\Gamma_{\bar{\mathrm{p}}}^{\mathrm{ann}}$ is defined as

$$\Gamma_{\bar{\mathrm{p}}}^{\mathrm{ann}} = \sigma_{\bar{\mathrm{p}}\mathrm{H}}^{\mathrm{ann}} v_{\bar{\mathrm{p}}} n_{\mathrm{H}} + \sigma_{\bar{\mathrm{p}}\mathrm{He}}^{\mathrm{ann}} v_{\bar{\mathrm{p}}} n_{\mathrm{He}}. \quad (6)$$

The annihilation cross section $\sigma_{\bar{\mathrm{p}}\mathrm{H}}^{\mathrm{ann}}$ is borrowed from [22,23] and we have multiplied it by a factor of $4^{2/3} \sim 2.5$, taking into account the higher geometric cross section, to get $\sigma_{\bar{\mathrm{p}}\mathrm{He}}^{\mathrm{ann}}$. The average hydrogen and helium densities in the galactic disk have been set equal to $n_{\mathrm{H}} = 0.9\ \mathrm{cm}^{-3}$ and $n_{\mathrm{He}} = 0.1\ \mathrm{cm}^{-3}$, respectively.

(iii) The annihilation of DM candidate particles throughout the Milky Way halo generates primary antiprotons. The corresponding source term $q_{\bar{\mathrm{p}}}^{\mathrm{prim}}(r, z, E)$ will be discussed in Sec. IV. Notice that annihilations take place all over the diffusive halo.

(iv) The latter is not the case neither for secondary antiprotons—which are produced as high-energy primary nuclei impinge on the atoms of the interstellar medium inside the galactic disk—nor for tertiary antiprotons which result from the inelastic and nonannihilating interactions which these particles may undergo with the same atoms. Antiprotons may actually collide on a proton at rest and transfer enough energy to excite it as a Δ resonance. This mechanism redistributes antiprotons towards lower energies and flattens their spectrum [13].

The rate for the production of secondary antiprotons, $q_{\bar{\mathrm{p}}}^{\mathrm{sec}}(r, E_{\bar{\mathrm{p}}})$, is discussed in more detail in Sec. III; for tertiary antiprotons, it is given by

$$q_{\bar{\mathrm{p}}}^{\mathrm{ter}}(r, E_{\bar{\mathrm{p}}}) = \int_{E_{\bar{\mathrm{p}}}}^{+\infty} \frac{d\sigma_{\bar{\mathrm{p}}\mathrm{H}\to\bar{\mathrm{p}}\mathrm{X}}}{dE_{\bar{\mathrm{p}}}}(E'_{\bar{\mathrm{p}}} \to E_{\bar{\mathrm{p}}}) n_{\mathrm{H}} v'_{\bar{\mathrm{p}}} \psi_{\bar{\mathrm{p}}}(r, E'_{\bar{\mathrm{p}}}) dE'_{\bar{\mathrm{p}}} - \sigma_{\bar{\mathrm{p}}\mathrm{H}\to\bar{\mathrm{p}}\mathrm{X}}(E_{\bar{\mathrm{p}}}) n_{\mathrm{H}} v_{\bar{\mathrm{p}}} \psi_{\bar{\mathrm{p}}}(r, E_{\bar{\mathrm{p}}}), \quad (7)$$

where the inelastic and nonannihilating differential cross section in this expression can be approximated by

$$\frac{d\sigma_{\bar{\mathrm{p}}\mathrm{H}\to\bar{\mathrm{p}}\mathrm{X}}}{dE_{\bar{\mathrm{p}}}} = \frac{\sigma_{\bar{\mathrm{p}}\mathrm{H}\to\bar{\mathrm{p}}\mathrm{X}}}{T'_{\bar{\mathrm{p}}}}. \quad (8)$$

Here, $T'_{\bar{\mathrm{p}}}$ is the initial antiproton kinetic energy. In order to take into account elastic scattering on helium, one simply has to replace the hydrogen density by $n_{\mathrm{H}} + 4^{2/3} n_{\mathrm{He}}$. With all these source terms specified, the full expression for the master equation describing the (Bessel transformed) antiproton distribution function $\bar{P}_i(z, E)$ becomes

$$\partial_z(V_C \bar{P}_i) - K\partial_z^2 \bar{P}_i + K\left\{\frac{\alpha_i^2}{R^2}\right\}\bar{P}_i + 2h\delta(z)\partial_E\{b^{\mathrm{loss}}(E)\bar{P}_i - K_{EE}(E)\partial_E \bar{P}_i\} = -2h\delta(z)\Gamma_{\bar{\mathrm{p}}}^{\mathrm{ann}}\bar{P}_i + Q_{\bar{\mathrm{p}},i}^{\mathrm{prim}}(z, E) + 2h\delta(z)\{Q_{\bar{\mathrm{p}},i}^{\mathrm{sec}} + Q_{\bar{\mathrm{p}},i}^{\mathrm{ter}}\}. \quad (9)$$

Integrating this relation along the vertical axis z—in particular through the infinitely thin disk—finally leads to a diffusion equation in energy which the Bessel transforms $\bar{P}_i(0, E)$ fulfill:

$$\bar{\mathcal{A}}_i \bar{P}_i(0, E) + 2h\partial_E\{b^{\mathrm{loss}}(E)\bar{P}_i(0, E) - K_{EE}(E)\partial_E \bar{P}_i(0, E)\} = 2h\{Q_{\bar{\mathrm{p}},i}^{\mathrm{sec}} + Q_{\bar{\mathrm{p}},i}^{\mathrm{ter}}\} + 2\int_0^L dz Q_{\bar{\mathrm{p}},i}^{\mathrm{prim}}(z, E) e^{-(V_C z/2K)} \mathcal{F}_i(z). \quad (10)$$

The coefficients $\bar{\mathcal{A}}_i$ that appear in the above expression are given by

$$\bar{\mathcal{A}}_i(E) = V_C + 2h\Gamma_{\bar{\mathrm{p}}}^{\mathrm{ann}}(E) + K(E) S_i \coth\left(\frac{S_i L}{2}\right), \quad (11)$$

where $S_i^2 = (V_C/K)^2 + (2\alpha_i/R)^2$, and the vertical functions $\mathcal{F}_i(z)$ are defined as

$$\mathcal{F}_i(z) = \sinh\left\{\frac{S_i}{2}(L - z)\right\} \Big/ \sinh\left\{\frac{S_i}{2} L\right\}. \quad (12)$$

In this work, we solve Eq. (10) by following the method explained in Appendix B of [5].

A completely different approach to describe the antiproton propagation through the diffusive halo relies on the existence of a Green function $G_{\bar{\mathrm{p}}}$. Such a function translates the probability for an antiproton produced at point $S(x_S, y_S, z_S)$ to travel to the observer located at point $M(x, y, z)$. The antiproton energy spectrum is given by the convolution of the Green function $G_{\bar{\mathrm{p}}}$ with the production rate $q_{\bar{\mathrm{p}}}$:

$$\psi(M, E) = \int d^3\mathbf{x}_S G_{\bar{\mathrm{p}}}(M \leftarrow S, E) q_{\bar{\mathrm{p}}}(S, E). \quad (13)$$

Energy loss, diffusive reacceleration, and tertiary produc-

tion are inefficient above a few GeV. For our purposes, we may therefore neglect these processes when deriving the antiproton propagator $G_{\bar{p}}$. The Milky Way is now pictured as an infinite slab of half-thickness L with a gaseous disk in the middle at $z = 0$. The antiproton propagation is invariant under a translation along the horizontal axis x or y. The master equation (3) needs still to be solved along the vertical direction z with the condition that $G_{\bar{p}}$ vanishes at the boundaries $z = \pm L$. The construction of the Green function for antiprotons is inspired from the positron case—see, in particular, Sec. 3 of [24]—with the difference that the antiproton energy does not change and that time is integrated out. Explicit expressions for $G_{\bar{p}}$ may be found in Appendix C.3.a of [25]. Because we are interested in the flux at the earth—i.e. within the disk, at $z = 0$—the integral (13) may be recast into

$$\psi(x_\odot = r_\odot, y_\odot = 0, z_\odot = 0, E) = 4\pi \int_0^L dz_S \int_0^R r_S dr_S G_{\bar{p}}(\odot \leftarrow S, E) q_{\bar{p}}(S, E), \quad (14)$$

where the antiproton propagator simplifies in that case into the series

$$G_{\bar{p}}(\odot \leftarrow S, E) = \frac{e^{-z_S/r_w}}{2\pi K(E)} \sum_{n=1}^{+\infty} \frac{1}{C_n} \phi_n(0)\phi_n(z_S) K_0\left(\frac{r}{L}\sqrt{\epsilon_n}\right). \quad (15)$$

Here, the vertical functions ϕ_n are given by

$$\phi_n(z) = \sin\left\{\xi_n\left(1 - \frac{z}{L}\right)\right\}, \quad (16)$$

where the coefficients ξ_n are solutions to the equation

$$\xi_n = n\pi - \tan^{-1}(p\xi_n). \quad (17)$$

At a given antiproton energy E, two specific scales may be singled out; the scattering length $r_s^{-1} \equiv h\Gamma_{\bar{p}}^{\rm ann}(E)/K(E)$ and a convective scale $r_w^{-1} \equiv V_C/2K(E)$. The parameter

$$\frac{1}{p} \equiv \frac{L}{r_s} + \frac{L}{r_w} \quad (18)$$

then serves to compare these two. At high energies, above $\sim$100 GeV, r_s and r_w are much larger than L due to the greatly enhanced diffusion coefficient $K(E)$. As a consequence, we have $p \gg 1$ and thus $\xi_n \approx (n - 1/2)\pi$. The scale C_n, defined by

$$\frac{C_n}{L} = 1 + \frac{1}{p}\left(\frac{\sin\xi_n}{\xi_n}\right)^2, \quad (19)$$

tends to L in this regime where p is large, i.e. when diffusion takes over disk annihilations and galactic convection. In the argument of the modified Bessel functions of the second kind K_0 in Eq. (15), the ratio r/L is multiplied by a factor $\sqrt{\epsilon_n}$, where

$$\epsilon_n = \xi_n^2 + \left(\frac{L}{r_w}\right)^2, \quad (20)$$

which reduces to ξ_n^2 in the pure diffusive regime at high energy.

As demonstrated later in more detail, the Bessel expansion and the propagator approach give similar results. The small discrepancies between the two methods will be discussed in Sec. IV but we may already now safely use Eq. (15) to get a deeper insight into antiproton propagation. In particular, we see that at high energies, the diffusion coefficient $K(E)$ in front of the expansion (15) is the only term that depends on the energy E. In the following section, we will return to this observation when we discuss the expected antiproton background at high energies.

III. THE ANTIPROTON BACKGROUND

Secondary antiprotons are produced by the spallation of the interstellar gas of the Milky Way disk—mostly hydrogen and helium—by impinging cosmic-ray primaries. In the case of the interactions between cosmic-ray protons and hydrogen atoms, the source term takes the following form:

$$q_{\bar{p}}^{\rm sec}(r, E_{\bar{p}}) = \int_{E_{\bar{p}}^0}^{+\infty} \frac{d\sigma_{pH\to\bar{p}}}{dE_{\bar{p}}}\{E_p \to E_{\bar{p}}\} n_H v_p \psi_p(r, E_p) dE_p. \quad (21)$$

The proton and helium cosmic-ray fluxes at the Earth have been measured accurately and have been borrowed from [5]. For each cosmic-ray model, they have been consistently propagated backward in the whole diffusive halo in order to yield $\psi_p(r, E_p)$ and $\psi_{He}(r, E_{nuc} = E_p)$. For kinematic reasons, the production rate peaks around a few GeV; this is because the proton energy must be larger than a threshold of $E_p^0 = 7m_p$. In the galactic frame, the differential production cross section that enters in the previous relation is given by the integral

$$\frac{d\sigma}{dE_{\bar{p}}} = 2\pi k_{\bar{p}} \int_0^{\theta_{\rm max}} \left(E_{\bar{p}} \frac{d^3\sigma}{d^3k_{\bar{p}}}\right)_{\rm LI} d(-\cos\theta), \quad (22)$$

where θ denotes the angle between the momenta of the incoming proton and the produced antiproton. In the center of mass (CM) frame, which drifts with a velocity $\beta_{\rm CM} = \{(E_p - m_p)/(E_p + m_p)\}^{1/2}$ with respect to the galactic frame, the antiproton energy cannot exceed a value of

$$E_{\bar{p},\rm max}^* = \frac{s - 9m_p^2 + m_{\bar{p}}^2}{2\sqrt{s}}, \quad (23)$$

where $\sqrt{s} = \{2m_p(E_p + m_p)\}^{1/2}$ is the total energy of the reaction. In Eq. (22), the energies E_p and $E_{\bar{p}}$ have been fixed and the angular integral runs from $\theta = 0$ up to a maximal value of $\theta_{\rm max}$ for which

$$\cos\theta_{\max} = \frac{1}{\beta_{\rm CM} k_{\bar{\rm p}}}\left(E_{\bar{\rm p}} - \frac{E^*_{\bar{\rm p},\max}}{\Gamma_{\rm CM}}\right). \qquad (24)$$

The Lorentz invariant differential cross section $E_{\bar{\rm p}}(d^3\sigma/d^3k_{\bar{\rm p}})$ depends on the antiproton rapidity $y = \tanh^{-1}(k_{\bar{\rm p}\|}/E_{\bar{\rm p}})$ and transverse mass $m_{\rm T}^2 = m_{\rm p}^2 + k_{\bar{\rm p}\perp}^2$; it has been parametrized according to [22,23]. In order to avoid numerical problems in the computation of (22), it is convenient to change the integration variable from $\theta_{\max}$ to $m_{\rm T}$ for small angles $\theta_{\max}$.

So far, we have discussed the spallation of hydrogen by high-energy protons. Let us now turn to helium, which is also present in both the cosmic radiation as well as in the interstellar material of the galactic disk. As regards the spallation of interstellar helium by cosmic-ray protons, the derivation of the differential cross section $d\sigma/dE_{\bar{\rm p}}({\rm pHe} \to \bar{\rm p})$ follows the same lines as explained above. Because the incoming proton interacts with a single nucleon of the target nucleus, the center of mass frame of the collision is the same as before. The Lorentz invariant differential cross section—which is the only new ingredient—has been parametrized in [26] as a function of $\sqrt{s}$, $k_{\bar{\rm p},\perp}$ and the ratio $x_R = E^*_{\bar{\rm p}}/E^*_{\bar{\rm p},\max}$. The total inelastic cross section for $p + A$ collisions is taken from [27]; a boost is then necessary to cope with the collisions of high-energy helium nuclei on interstellar hydrogen. An antiproton with rapidity y in the reference system of the hydrogen target has a rapidity $-y' = \cosh^{-1}(E_{\rm nuc}/m_{\rm p}) - y$ in the reference frame of the impinging helium nucleus. The integral (21) runs now over the energy per nucleon $E_{\rm nuc}$ of the incident cosmic-ray He. Finally, because helium amounts to a fraction of ~0.1 with respect to hydrogen, we expect He + He interactions to contribute only a few percent to the secondary antiproton flux. Inspired by [28], we have multiplied the differential cross section $d\sigma/dE_{\bar{\rm p}}({\rm pHe} \to \bar{\rm p})$ by the effective number η of nucleons inside the impinging He nucleus that participate in the reaction. It is given by the ratio of the average number $\langle n_{\rm int}\rangle$ of nucleon-nucleon interactions over the average number $\langle n_{\rm T}\rangle$ of target nucleons involved. Both $\langle n_{\rm int}\rangle$ and $\langle n_{\rm T}\rangle$ depend on the center of mass energy. At $\sqrt{s} = 10$ GeV for instance, we have $\langle n_{\rm int}\rangle = 3.68$ and $\langle n_{\rm T}\rangle = 2.64$, thus leading to $\eta = 1.39$. This value increases up to $\eta = 5.12/3.25 = 1.58$ at $\sqrt{s} = 1$ TeV, not too far from the simple scaling factor of $A^{1/3} = 1.59$ which we have used in our code.

In Fig. 1, the various contributions to the secondary antiproton flux, $\Phi = v\psi/4\pi$, from the spallation of interstellar H and He by cosmic-ray protons and alpha particles are presented together with the existing low-energy data. Galactic propagation parameters corresponds to the "medium" configuration of Table I, to be discussed later. Solar modulation has been implemented through the force field approximation [29], with a Fisk potential $\phi_{\rm F}$ of 500 MV corresponding to the minimum of solar activity during which the observations have been performed. Above an

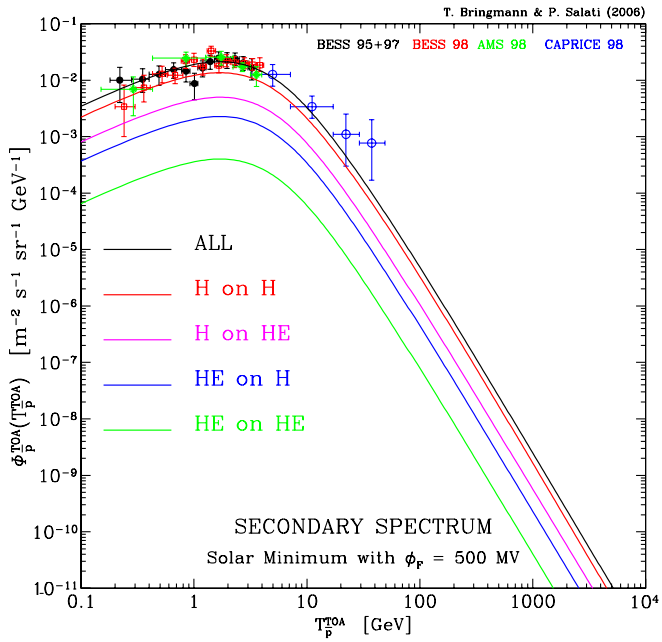

FIG. 1 (color online). The various contributions to secondary antiprotons from the spallation of the interstellar medium by cosmic rays. Here, we took the medium configuration of propagation parameters from Table I and $T_{\bar{p}}^{\rm TOA}$ denotes the antiproton kinetic energy as measured at the top of the atmosphere. For reference, we also show the existing low-energy data on the antiproton flux at the top of the atmosphere [1–4].

energy of a few tens of GeV, the antiproton flux decreases like a power law. If the scaling violations of the differential production cross section $d\sigma/dE_{\bar{\rm p}}$ were negligible, the secondary source term $q_{\bar{\rm p}}^{\rm sec}(r, E)$ would have the same energy dependence as the impinging cosmic-ray flux $\Phi = v\psi/4\pi \propto E^{-\gamma}$. As discussed at the end of Sec. II, the antiproton propagator $G_{\bar{\rm p}}$ scales at high energy like $1/K \propto E^{-\delta}$. We expect the antiproton flux to have a typical spectral behavior like $G_{\bar{\rm p}} \times \Phi \propto E^{-\gamma-\delta}$. The cosmic-ray proton and helium fluxes have been borrowed from [5] where a fit of the BESS [30] and AMS [31] data is featured. The spectral index γ is found to be equal to 2.72 for protons and to 2.74 for helium. Would hadronic interactions be scale invariant, the secondary antiproton flux of Fig. 1—for which $\delta = 0.7$—would drop like $\sim E^{-3.4}$. The actual

TABLE I. Typical combinations of diffusion parameters that are compatible with the B/C analysis [6]; as demonstrated later, these parameter sets correspond to minimal, medium, and maximal primary antiproton fluxes, respectively.

Case	δ	K_0 [kpc^2/Myr]	L [kpc]	V_C [km/s]	V_a [km/s]
Maximal	0.46	0.0765	15	5	117.6
Medium	0.70	0.0112	4	12	52.9
Minimal	0.85	0.0016	1	13.5	22.4

spectrum is slightly harder with an $E^{-3.3}$ energy dependence. As a cross-check, we also took for comparison the parametrization of [26] (instead of [22,23]) for the antiproton production cross section through $pH \rightarrow \bar{p}X$. In this case we find qualitatively the same spectrum, with a slightly harder spectral index of 3.2 instead of 3.3. This corresponds to an uncertainty in the background flux which is much smaller than the one induced by the not fully determined propagation parameters—see the discussion below.

The semianalytic treatment of cosmic-ray propagation that is based on the Bessel expansion (4) is a convenient framework to derive the theoretical uncertainties associated to the various parameters at stake—namely K_0, δ, V_a, V_C, and the thickness L. The space of these propagation parameters has been extensively scanned [6] in order to select the allowed regions where the predictions on B/C—a typical cosmic-ray secondary to primary ratio—match the observations. Several hundreds of different propagation models have survived that crucial test. The propagation parameters are thus only loosely constrained by the cosmic-ray nuclei abundances so far observed. The same conclusion has been reached independently in Ref. [32] with the help of a fully numerical code [33] in which the convective wind V_C increases linearly with vertical height z. However, the B/C ratio could not be accounted for when both galactic convection and diffusive reacceleration were implemented at the same time, a problem which our Bessel treatment does not encounter.

The yellow band shown in Fig. 2 is the envelope of the secondary antiproton spectra computed with the set of ~1600 different propagation models found in [6] to pass the B/C test. This band comprises the theoretical uncertainty in the determination of the secondary antiproton flux. It is confined by the ''minimal'' and ''maximal'' configurations of Table I. As a first observation, we notice how narrow the uncertainty strip is between ~10 and 100 GeV. The PAMELA and AMS-02 collaborations will thus be able to highlight even small spectral deviations in that energy range. Above ~100 GeV, the yellow band widens as a result of the energy dependence of the diffusion coefficient K: from the B/C analysis, the spectral index δ may take any value between 0.46 and 0.85; its spread $\Delta\delta = 0.4$ thus translates into a factor of $10^{0.8} \sim 6$ of uncertainty on the antiproton flux at 10 TeV—two decades above the energy where the yellow strip is still the thinnest. In fact, we see this expectation confirmed in the right panel of Fig. 2, where we can read off a ratio of 1 to 6 (at 10 TeV) between the minimal and maximal antiproton flux expectations. This large uncertainty in the secondary antiproton background at TeV energies may look depressing. One should keep in mind, however, that PAMELA and AMS-02 will considerably improve the measurements of the cosmic-ray nuclei abundances with a determination of the B/C ratio to a better accuracy and over a wider energy range than available so far. This will translate into improved constraints on the propagation parameters and eventually into a thinner uncertainty strip in the panels of Fig. 2. The antiproton spectrum itself will also be measured up to a few TeV in the case of AMS-02. Once it is compared to the cosmic-ray proton and helium fluxes, the spectral index δ should be better determined. Finally, we expect the LHC to improve the accuracy of the antiproton production cross sections of the various nucleus-nucleus interactions at stake. When going to very high energies, a word of caution is nevertheless mandatory. The antiproton flux rapidly decreases with energy and becomes vanishingly small above 1 TeV. Even with the AMS-02 large acceptance, the statistical error on a measurement of the antiproton background at ~800 GeV is comparable to the present theoretical uncertainty as featured in the left panel of Fig. 7: the vertical error bars of the highest energy data point extend over the yellow uncertainty strip. In fact, above 10 TeV we expect not more than

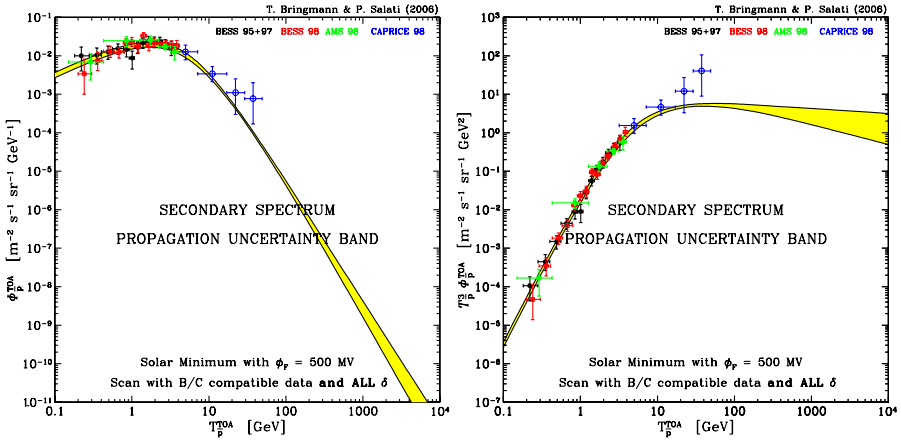

FIG. 2 (color online). Theoretical uncertainties in the secondary flux in antiprotons, taking into account the whole range of propagation parameters that is allowed by the existing B/C data, again featured together with the existing low-energy data. In the right panel of this figure, we have plotted $T_{\bar{p}}^3 \Phi_{\bar{p}}$ in order to better illustrate the expected near $T_{\bar{p}}^{-3}$ scaling of the flux at high energies.

$\mathcal{O}(1)$ antiprotons per m^2 and *year*, posing a formidable (if surmountable) challenge even for follow-up experiments. In this article, we therefore restrict our analysis throughout to an energy range $\lesssim 10$ TeV.

IV. ANTIPROTONS FROM DARK MATTER ANNIHILATIONS IN THE GALACTIC HALO

The source function $q_{\bar{\mathrm{p}}}^{\mathrm{prim}}(T, \mathbf{r})$ describes the number of primary antiprotons per unit time, energy, and volume element that are produced with a kinetic energy T at a given position $\mathbf{r}$ in the galactic halo:

$$q_{\bar{\mathrm{p}}}^{\mathrm{prim}}(T, \mathbf{r}) = \frac{1}{2}\langle\sigma_{\mathrm{ann}}\upsilon\rangle\left\{\frac{\rho_{\mathrm{CDM}}(\mathbf{r})}{m}\right\}^2 \sum_f B^f \frac{\mathrm{d}N^f}{\mathrm{d}T}. \quad (25)$$

Here, $\langle\sigma_{\mathrm{ann}}\upsilon\rangle$ is the DM self-annihilation rate, ρ_{CDM} the DM halo density and m the DM particle's mass. The sum runs over all annihilation channels f, where B^f are the branching ratios and $\mathrm{d}N^f/\mathrm{d}T$ the fragmentation functions into antiprotons, respectively. The factor of $1/2$ has to be included whenever the DM particle is its own antiparticle and therefore only annihilates in pairs (which is the case for the DM candidates that we will consider below).

The source function can thus be disentangled into an astrophysical part, given by the dark matter distribution ρ_{CDM}, and a particle physics part that comprises the remaining information. The first one is usually subject to much greater uncertainties than the latter and will be dealt with in the following subsection. In Sec. IV B, we will then address the particle physics part by discussing three benchmark scenarios with DM masses in the TeV range, with their respective expressions for the annihilation cross section and branching ratios. The fragmentation functions $\mathrm{d}N^f/\mathrm{d}T$, finally, can be obtained from Monte Carlo programs like PYTHIA [34]. We use here the tabulated fragmentation functions of the DARKSUSY package [35], which are based on a large number of PYTHIA runs (10^6 per annihilation channel and mass).

A. The distribution of dark matter in the Milky Way

1. Halo profiles

The Milky Way halo distribution is only poorly constrained by direct observations and its form must therefore be inferred from N-body simulations of gravitational clustering. Because of the restricted resolution of these simulations, however, the innermost slope of the density profile can only be obtained by an extrapolation of the behavior at larger radii (i.e. $r \gtrsim 0.1$ kpc) and is thus bound to a considerable amount of uncertainty; furthermore, it is still an (numerically) unsolved issue how to correctly include the effect of baryons during the gravitational collapse. To account for this situation, we will here for illustrative purposes restrict ourselves to a choice of four different profiles that basically span the whole range of reasonable halo models with respect to indirect dark matter detection prospects; the isothermal sphere, the Navarro-Frenk-White (NFW) [36], and the Moore profiles [37,38]. Like most of their relatives, these halo models can be parametrized as

$$\rho_{\mathrm{CDM}}(\mathbf{r}) = \rho_{\mathrm{s}}\left(\frac{r_{\mathrm{s}}}{r}\right)^{\gamma}\left\{1 + \left(\frac{r}{r_{\mathrm{s}}}\right)^{\alpha}\right\}^{(\gamma-\beta)/\alpha}, \quad (26)$$

where the corresponding parameters are summarized in Table II. Note that at the Sun's distance to the galactic center, $r = R_0 \equiv 8.5$ kpc, one recovers for all profiles a local halo density of $\rho_0 = \rho_{\mathrm{CDM}}(R_0) \sim 0.3\ \mathrm{GeV\,cm^{-3}}$.

Our semianalytic treatment of cosmic-ray galactic propagation relies on Bessel expansions like (4). The function $J_0(\alpha_i r/R)$ probes details as small as $\lambda \sim 2\pi R/\alpha_i$, where α_i is the ith zero of the function J_0 and R denotes the radius of the diffusive halo. In the case of an NFW or Moore profile, the correct description of the central cusp—where the annihilation rate diverges like $r^{-2\gamma}$—would imply the necessity of an infinite series of such Bessel functions. This would lead to unacceptable CPU time and to a lack of numerical accuracy. Following the method explained in [42], we have renormalized the DM central distribution without modifying the absolute number of DM particle annihilations. Actually, within a small sphere of radius r_c, we have replaced the density profile (26) which diverges like $\rho(r)/\rho_c = (r_c/r)^{\gamma}$, where $\rho_c \equiv \rho(r_c)$, by the milder distribution

$$\left\{\frac{\rho(r \le r_c)}{\rho_c}\right\}^2 = 1 + \left\{\frac{2\pi^2}{3}(\xi - 1)\mathrm{sin}_c^2\left(\frac{\pi r}{r_c}\right)\right\}, \quad (27)$$

where $\mathrm{sin}_c(x) \equiv \sin(x)/x$. That renormalized density leads to the same number of DM annihilations as the actual cusp provided that

$$\xi = \frac{3}{3 - 2\gamma}, \quad (28)$$

in the case of NFW 97 and Moore 04. Note that for the

TABLE II. Parameters in Eq. (26) for the halo models that we consider here. Scale radius r_{s} and density ρ_{s} are strongly correlated with the virial mass of the galaxy [39] and we adopt the values obtained in [40] for the Milky Way. In the case of the Moore 99 profile, DM self-annihilations set an upper bound to the maximal possible density and we follow the usual prescription of imposing a cutoff radius inside which ρ_{CDM} is assumed to be constant [41]. When the DM distribution is cuspy—for $\gamma \ge 1$—we smooth it so as to keep the total number of annihilations constant—see the text for further details.

Halo model	α	β	γ	ρ_{s} $[10^6 M_\odot\ \mathrm{kpc}^{-3}]$	r_{s} [kpc]
Isothermal sphere	2	2	0	7.90	4
NFW 97 [36]	1	3	1	5.38	21.75
Moore 04 [37]	1	3	1.16	2.54	32.62
Moore 99 [38]	1.5	3	1.5	1.06	34.52

Moore 99 cusp, the actual annihilation rate diverges logarithmically and we have to impose a cutoff on the DM density, $\rho_{\rm CDM} \lesssim \rho_{\rm ann}$. This upper bound arises from the increasing DM self-annihilation rate in regions of enhanced DM densities and is given by

$$\rho_{\rm ann} = \frac{m}{\langle \sigma_{\rm ann} v \rangle \tau}, \tag{29}$$

where an age of $\tau = 12$ Gy has been assumed for the central DM concentration. This cutoff translates into a factor of

$$\xi_{\rm Moore99} = 2 \ln\left(\frac{\rho_{\rm ann}}{\rho_c}\right). \tag{30}$$

In practice, we have set $r_c = 500$ pc and pushed the Bessel expansion up to the 200th order. We have accelerated its convergence by using the method explained in [43]. Because the antiproton propagator $G_{\bar{\rm p}}$ that connects the solar system to the galactic center varies smoothly over that region, a smaller core radius r_c would not appreciably change our results.

2. Boost factors

Following the paradigm of hierarchical structure formation, it is very likely that the DM distribution exhibits substructures (''clumps''), i.e. small inhomogeneities superimposed on the smooth background profiles described above. On very small scales, e.g., one expects a cutoff in the cold dark matter power spectrum [44] and a considerable number of the first gravitationally bound objects, with a mass around this cutoff, might have survived until today [45]. Another interesting proposal is the existence of a population of intermediate mass black holes (IMBHs) in our galaxy, each of them being surrounded by a DM mini-halo with a rather steep profile, i.e. a ''mini-cusp'' [46]. The effect of halo substructures is in any case to enhance the flux of antiprotons—or any other primarily produced particles—at earth, as compared to the case of a smooth DM matter distribution. Such an enhancement immediately follows from the fact that $\langle \rho^2 \rangle$ is generally larger than $\langle \rho \rangle^2$, with the difference increasing with the degree of inhomogeneity, and is often encoded in a universal boost factor b. However, as has been stressed in [24], this boost factor is actually not so universal in that it—given a DM distribution $\rho_{\rm CDM}$—depends on both the particle species and the energy range under consideration (see, e.g., [20] for a similar observation).

As an example, and as a practical application of the formalism developed in [24], let us now determine the boost factor for antiprotons in the ''type B'' IMBH scenario of [46]—which is representative of a class of models in which black holes originate from massive objects formed directly during the collapse of primordial gas in early-forming halos. A complete discussion of the antiproton signal and of its statistical properties is not in the focus of this paper and the reader is rather referred to the thorough analysis of Ref. [47] for details. As a sneak preview of that work, we derive here the effective boost factor

$$B_{\rm eff} = \frac{\langle \Phi_{\bar{\rm p},\rm IMBH} \rangle}{\Phi_{\bar{\rm p},\rm smooth}}, \tag{31}$$

for an average IMBH population of type B. A smooth halo density $\rho_{\rm CDM}$ yields a flux

$$\Phi_{\bar{\rm p},\rm smooth} \propto \int d^3\mathbf{x}_S G_{\bar{\rm p}}(M \leftarrow S, E) \left\{\frac{\rho_{\rm CDM}(\mathbf{r})}{\rho_0}\right\}^2, \tag{32}$$

whereas the IMBH contribution is given by

$$\langle \Phi_{\bar{\rm p},\rm IMBH} \rangle \propto \int d^3\mathbf{x}_S G_{\bar{\rm p}}(M \leftarrow S, E) \xi_{\rm sp} n_{\rm sp}(\mathbf{r}). \tag{33}$$

In Ref. [47], the average number $n_{\rm sp}$ of mini-spikes per unit volume has been fitted with the results of $\sim$200 different Monte Carlo realizations—each containing eventually a hundred objects—obtained in Ref. [46] by evolving an initial distribution of IMBHs orbiting in the galactic halo and by taking into account close encounters and their associated tidal disruptions. The enhancement of the DM annihilation rate inside each mini-spike is described by the source boost factor

$$\xi_{\rm sp} = \int_{\rm DM\ cloud} \left\{\frac{\delta\rho_{\rm CDM}(\mathbf{r})}{\rho_0}\right\}^2 d\mathbf{r}, \tag{34}$$

where ρ_0 is some value of reference generally set equal to $\rho_{\rm CDM}(R_0)$. In a region of size $R_{\rm sp}$ around the IMBH, the DM density is described by a power law $r^{-7/3}$. The annihilation rate diverges at the center and we impose a cutoff on the DM density $\rho_{\rm CDM} \lesssim \rho_{\rm ann}$—see Eq. (29) and Ref. [41]. The effective volume $\xi_{\rm sp}$ depends on the DM particle mass m and self-annihilation cross section $\langle \sigma_{\rm ann} v \rangle$. We have used here an average spike radius of $R_{\rm sp} = 2.84$ pc and an average surface density of $\delta\rho_{\rm CDM}(R_{\rm sp}) = 48.51\ {\rm M}_\odot\ {\rm pc}^{-3}$—see once again Ref. [47] for details.

In the upper panels of Fig. 3, the isothermal sphere of Table II corresponds to the smooth distribution of reference with respect to which the enhancement of the antiproton signal is computed. A DM particle mass $m = 1$ TeV and a self-annihilation cross section $\langle \sigma_{\rm ann} v \rangle = 3 \times 10^{-24}\ {\rm cm}^3\ {\rm s}^{-1}$ lead to a mini-spike effective volume of $\xi_{\rm sp} = 1.2 \times 10^5\ {\rm kpc}^3$. In the lower panels where the isothermal sphere is replaced by an NFW profile, a DM particle mass of 1 TeV and a self-annihilation cross section of $3 \times 10^{-26}\ {\rm cm}^3\ {\rm s}^{-1}$ have been assumed, hence a value of $\xi_{\rm sp} = 3.1 \times 10^6\ {\rm kpc}^3$. In the left panels, cosmic-ray propagation does not include the contribution from tertiaries, nor energy losses and diffusive reacceleration. Switching off these processes allows one to perform the calculation of $B_{\rm eff}$ by the two methods presented in Sec. II. The convolution over the diffusive halo of the antiproton propagator $G_{\bar{\rm p}}$ with the square $\{\rho_{\rm CDM}(\mathbf{r})/\rho_0\}^2$ of the smooth DM

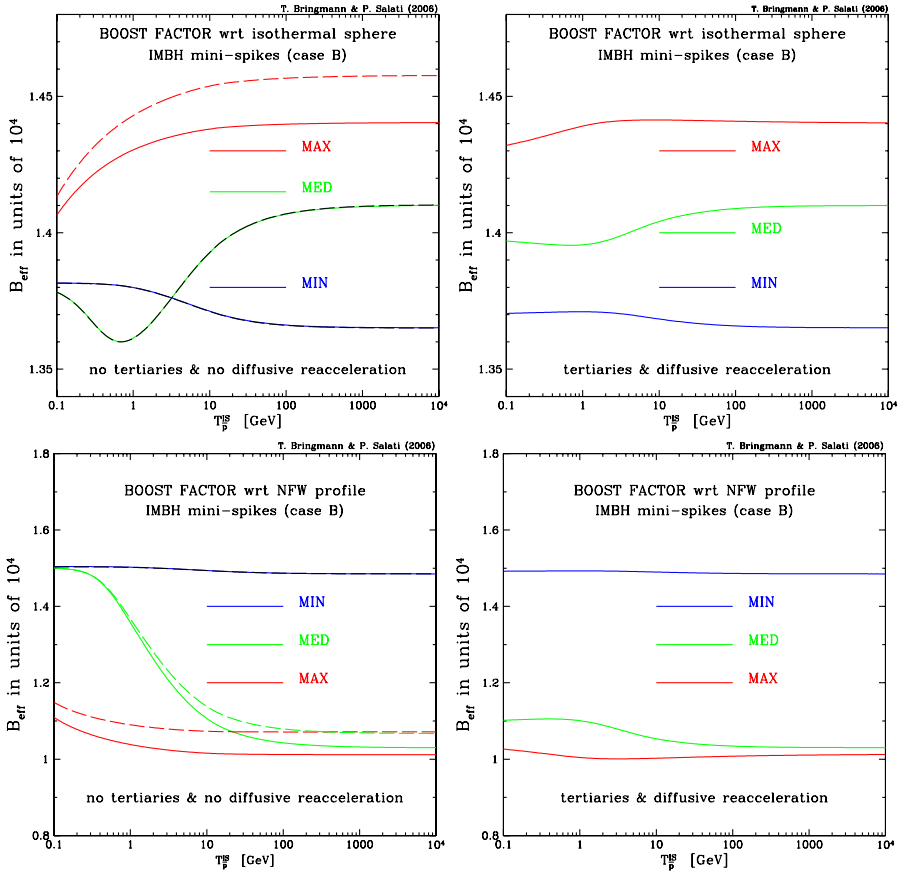

FIG. 3 (color online). Boost factor for an average Milky Way halo population of IMBHs as a function of the antiproton kinetic energy. The two panels on the left do not include the contribution from tertiaries, energy losses, and diffusive reacceleration. The long-dashed lines have been obtained by integrating directly the antiproton Green function $G_{\bar{p}}$ over the diffusive halo. In the right panels, tertiaries, energy losses, and diffusive reacceleration have been taken into account. An isothermal sphere (top panels) as well as an NFW profile (bottom panels) have been considered for the DM smooth distribution.

density profile (26) and with the IMBH source term $\xi_{\rm sp} n_{\rm sp}(\mathbf{r})$ leads to the long-dashed curves. Alternatively, we have directly included the IMBH source term $\xi_{\rm sp} n_{\rm sp}(\mathbf{r})$ in our Bessel code to generate the solid lines. The injection spectrum of antiprotons cancels out in the calculation. The agreement between these two different approaches is astonishingly good. The discrepancies do not exceed a few percent in the worst case. This occurs, in particular, for maximal propagation where the range of the antiproton propagation is large and allows one to probe the radial boundaries of the diffusive halo. In the Bessel approach, the cosmic-ray density vanishes at $r = R$. This condition is not implemented in the propagator approach even if the contribution of the outward regions is not taken into account. This leads to an overestimation of $B_{\rm eff}$ as is particularly clear in the upper-left panel. At first glance, the boost factor depends very weakly on the propagation model. As the antiproton energy increases, so does the propagation range. In the case of the isothermal sphere, the population of galactic IMBHs—whose number density is given on average by $n_{\rm sp}(\mathbf{r})$—tends to contribute more to the signal than the smooth distribution. As the propagation range increases, more and more mini-spikes come into play. This results into the increase of $B_{\rm eff}$ in the upper-left panel for the medium and maximal propagation configurations. On the contrary, in the case of an NFW profile, as soon as the propagation range reaches the galactic center and its strong DM annihilation site, the boost factor drops as is particularly clear for the medium configuration of the lower-left panel. In the right panels, tertiary production, energy losses, and diffusive reacceleration have been switched on with the consequence of smoothing the variations of the boost factor with energy. In Fig. 3, the values of $\xi_{\rm sp}$ have been adjusted in order to get a boost of $\sim 10^4$—though the DM particle mass and self-annihilation cross section are reasonable. Because the distribution of mini-spikes inside the galactic halo is not unique, the boost factor $B_{\rm eff}$ is subject to large variations—typically a factor of a few exceeding 10 at low antiproton energies—depending on the actual IMBH distribution. For a full analysis of the associated boost uncertainty, we refer to [47]—but would like to mention already here that we expect this variance to decrease significantly at the high energies considered here.

B. Dark matter masses at the TeV scale

Searching for possible primary contributions to the antiproton spectrum at very high energies, we have to focus on the annihilation of rather heavy (i.e. at least TeV scale) DM particles. While such high masses can appear in a variety of models, we will restrict ourselves in the following to the most popular and most commonly studied scenarios, i.e. supersymmetry and extra dimensions. In this section, we introduce the DM candidates that arise in these scenarios and in each case briefly describe the main features that are relevant in our context. First, however, note that the usual WIMP relation,

$$\Omega_{\rm WIMP} h^2 \sim \frac{3 \times 10^{-27}\ {\rm cm}^3\,{\rm s}^{-1}}{\langle \sigma v \rangle}, \tag{35}$$

in general rather prefers slightly smaller masses. To balance the reduced annihilation cross sections one expects for higher masses, one has thus to rely on the presence of effective coannihilation channels with other particles during the freeze-out process. In accordance with this observation, the mass splitting between the DM particle and the next-to-lightest nonstandard model particles is generically very small in all the examples described below.

Let us now start with the case of supersymmetry, where the lightest stable supersymmetric particle (LSP) provides an excellent dark matter candidate [10]. In most models, it is given by the (lightest) neutralino, which is a linear combination of the superpartners of the gauge and Higgs fields,

$$\chi \equiv \tilde{\chi}_1^0 = N_{11}\tilde{B} + N_{12}\tilde{W}^3 + N_{13}\tilde{H}_1^0 + N_{14}\tilde{H}_2^0. \tag{36}$$

While the neutralino is often a gaugino, with a large Bino fraction and a mass of a couple of hundred GeV or less, the hyperbolic branch/focus point region of minimal supergravity (mSUGRA) typically exhibits very heavy neutralinos with a large Higgsino fraction [16]. From the requirement that Higgsinos should give the right relic density, their mass has to be around 1 TeV [48]. For these high masses, the neutralino is an almost pure (anti)symmetric combination of the two neutral Higgsino states—in which case the annihilation cross section into Z (as well as into Higgs boson) pairs vanishes exactly and that into quarks is usually heavily suppressed by multi-TeV squark masses in the propagator. For these reasons the annihilation into W bosons typically clearly dominates; depending on the actual neutralino composition, however, a significant fraction can also go into Z bosons or heavy quark pairs.

Another interesting situation arises in the case of a neutralino that is almost a pure Wino, as expected, for example, in anomaly mediated supersymmetry breaking scenarios [49]. For Winos, the preferred mass from relic density requirements is peaked at about 1.7 TeV [48] (a *pure* Wino state obtains the right relic density for $m \sim$ 2.2 TeV; taking into account nonperturbative effects, this mass is further increased by about 600 GeV [50]). Nonperturbative, binding energy effects then result in greatly enhanced annihilation cross sections today, when the neutralinos have very small galactic velocities [17]. In this limit, heavy Winos annihilate almost exclusively into gauge bosons (as a side remark, the annihilation into photons is also significantly enhanced with respect to the nonperturbative result, leading to promising prospects for an indirect detection in terms of gamma rays [17,51,52]).

The third example of a TeV scale dark matter candidate we want to consider here is that of the LKP in models with universal extra dimensions [14], where all standard model fields are allowed to propagate in a higher-dimensional bulk. After compactification of the internal space, these additional degrees of freedom appear as towers of new, heavy states in the effective four-dimensional theory; the stability of the lightest of these states, i.e. the LKP, is guaranteed by the existence of an internal Z_2 symmetry (called KK parity) that derives from higher-dimensional translational invariance. Taking into account radiative corrections to the KK masses, the LKP is expected to be well approximated by the $B^{(1)}$, the first KK excitation of the weak hypercharge boson [15]. Detailed relic density calculations show that it can account for the required dark matter density if the compactification scale (and thus the $B^{(1)}$ mass) lies in the range $0.6 \lesssim m_{B^{(1)}} \lesssim 1.4$ TeV [53], mainly depending on the standard model Higgs mass; deviations from the minimal scheme for calculating the radiative mass spectrum weaken the upper bound on the compactification scale to about 2 or 3 TeV [54]. The main annihilation channels of the $B^{(1)}$ that are relevant for antiproton production are those into quark pairs (about 35% in total); the annihilation into gauge and Higgs bosons is of the order of 1% each and thus subdominant.

Finally, let us stress once more that, in all these examples of heavy WIMP candidates, TeV masses appear in a very natural way. Furthermore, one may easily find even higher masses for e.g. neutralino dark matter as soon as one leaves minimal prescriptions for supersymmetry breaking [55]. However, since the annihilation cross section in general scales as $\langle \sigma_{\rm ann} v \rangle \propto m^{-2}$, the number of primary antiprotons is suppressed as

$$q_{\bar{\rm p}}^{\rm prim} \propto m^{-4}. \tag{37}$$

This means that, even if the background flux scales roughly as T^{-3} (see Sec. III), it is very unlikely that one will be able to discriminate a primary antiproton contribution from DM particles with masses significantly higher than 1 TeV—unless one allows for artificially high boost factors.[1] Since

[1]Note that this argument can be evaded if one encounters resonant DM annihilations that still—as in the case of heavy Winos [17]—do not significantly alter the relic abundance.

TABLE III. Our benchmark models for studying possible primary contributions to the antiproton spectrum at high energies; m is the DM particle's mass (in TeV), $\langle\sigma_{\rm ann}v\rangle$ its annihilation rate (in 10^{-26} cm^3 s^{-1}) and the remaining columns give the branching ratios into the annihilation channels relevant for $\bar{p}$ production (in percent). The corresponding values are typical for high Higgsino (LSP1.0) and Wino (LSP1.7) fractions of the neutralino; for the latter we take the nonperturbative expressions from [17], while for the former we have calculated the annihilation cross section of a pure (anti)symmetric Higgsino into W bosons and choose to neglect other annihilation channels (see text for further details). In the case of the LKP, the quoted values for the branching ratios, as well as $\langle\sigma_{\rm ann}v\rangle m^2$, are actually very insensitive to the parameters of the model (see, e.g., [20]).

DM model	m	$\langle\sigma_{\rm ann}v\rangle$	$t\bar{t}$	$b\bar{b}$	$c\bar{c}$	$s\bar{s}$	$u\bar{u}$	$d\bar{d}$	ZZ	W^+W^-	HH	gg
LSP1.0	1.0	0.46								100		
LKP1.0	1.0	1.60	10.9	0.7	11.1	0.7	11.1	0.7	0.5	1.0	0.5	0.5
LSP1.7	1.7	102							20.1	79.9		
LKP1.7	1.7	0.55	11.0	0.7	11.1	0.7	11.1	0.7	0.5	0.9	0.5	0.5

also the total rates become very low far beyond 1 TeV, we do not consider such high DM masses in the following.

C. Future detectability

After having introduced typical scenarios with high DM masses, let us now choose as benchmark models a 1 TeV pure Higgsino, a 1.7 TeV pure Wino, and a $B^{(1)}$ with corresponding masses (having in mind, of course, a direct comparison between the LKP and the LSP). In Table III, we summarize the main properties of these DM candidates. Before we now proceed to study possible imprints in the antiproton spectrum for our benchmark models, we note

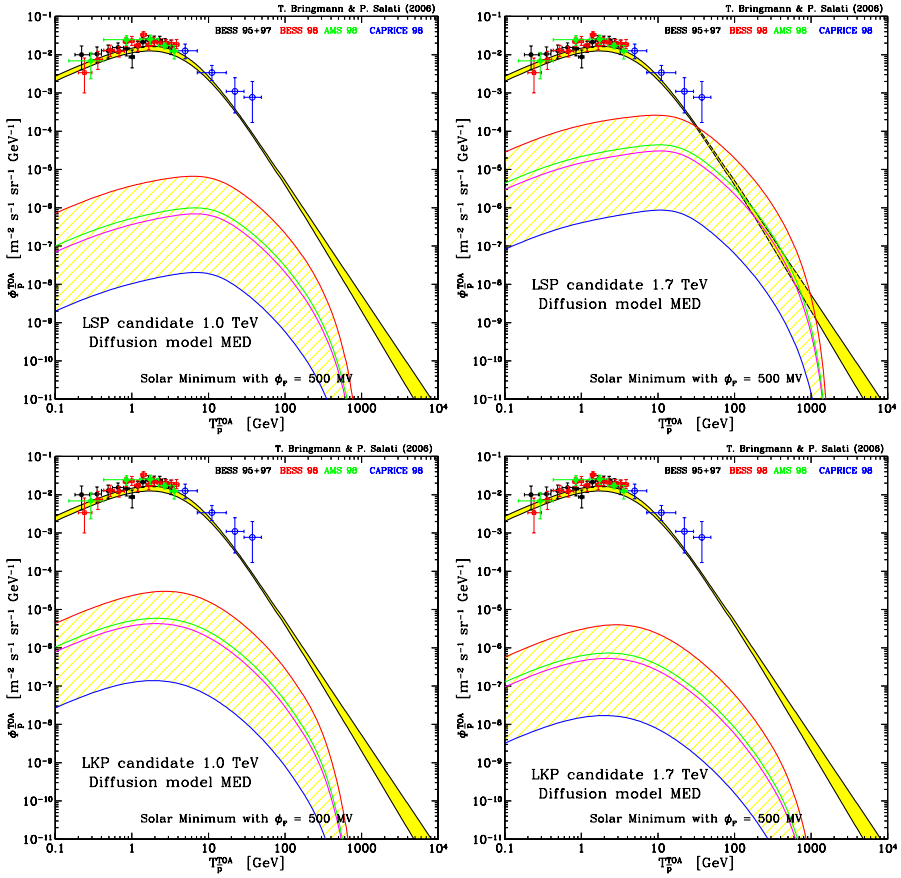

FIG. 4 (color online). The primary flux in antiprotons, as compared to the background in secondaries, for the set of benchmark models specified in Table III. From bottom to top, the different curves correspond to the isothermal sphere, NFW, Moore 04, and Moore 99 profiles, respectively; for the diffusion parameters we adopt the medium configuration of Table I.

that the cases of a pure Wino [21] and the LKP [20,42] have already attracted some attention before.

With the source function specified in Eq. (25), we can easily apply the formalism described in Sec. II to compute the corresponding primary flux of antiprotons. Let us start by showing in Figs. 4 and 5 the results for our benchmark models, for various halo profiles and diffusion parameters. Note first that the dependence on the halo profile is as usual much less severe than in the case of e.g. gamma rays, where the flux usually differs by several orders of magnitude for the profiles that we consider here; the simple reason for this, of course, is that the vast majority of antiprotons do not reach far enough through the diffusive halo to probe the very inner region of the galaxy, where the differences between the halo profiles are most pronounced. The dependence on the diffusion parameters, on the contrary, is rather strong—although the B/C constraints basically fix the secondary antiproton flux. This effect has been described before [5,56] and can be attributed to the fact that primary and secondary antiprotons mainly probe different regions of the halo. It clearly illustrates the need for cosmic-ray data that are both more accurate and span a larger energy range, each of which would greatly increase the predictability for primary contributions to the antiproton flux.

Unfortunately, the expected primary components are usually smaller than the background fluxes in secondary antiprotons even for favorable diffusion parameters—with the striking exception of the 1.7 TeV Wino, where the resonantly enhanced annihilation cross section may allow for a spectacular signal in the range of a few 100 GeV already for very conservative assumptions about the DM distribution (i.e. no boost factor at all). We can thus confirm the claim of [21] that Wino DM exhibits very promising observational prospects in terms of primary contributions to the antiproton flux.

However, let us now recall from our discussion in the preceding section that we actually do expect primary fluxes that are boosted with respect to what is shown in Figs. 4 and 5. As we have emphasized, even rather high boost factors are feasible and appear in several realistic scenarios. To illustrate this point, we plot in Fig. 6 the primary fluxes for our benchmark models—as before for an NFW profile and the diffusion parameter configurations of Table I, but this time in the presence of IMBHs. All of a sudden, the situation has drastically changed and a plethora

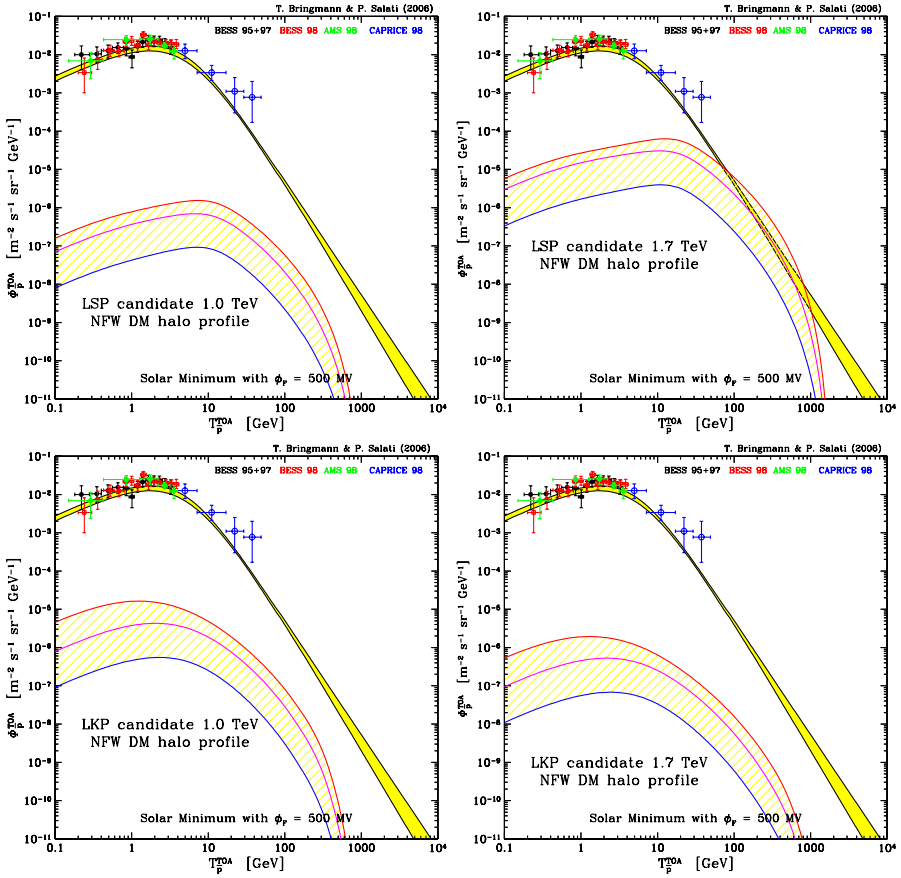

FIG. 5 (color online). Same as Fig. 4, now for an NFW halo profile; the diffusion parameters are varied from the minimal to the maximal configurations of Table I.

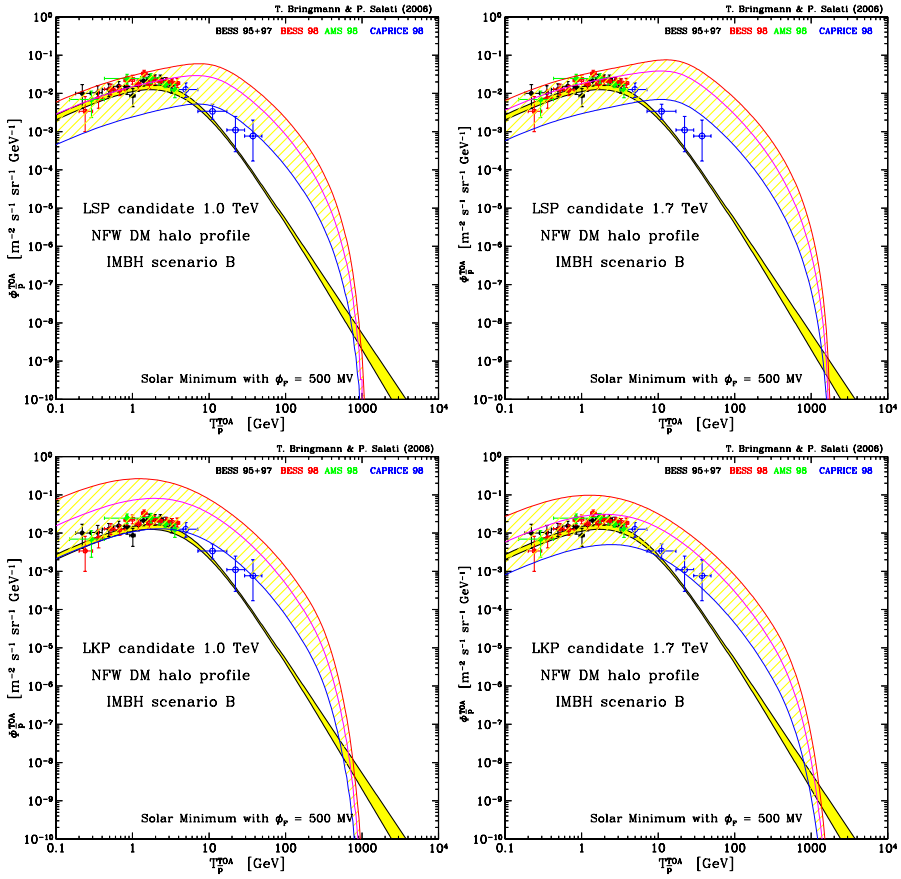

FIG. 6 (color online). Same as Fig. 5, now with an NFW profile and a typical population of IMBHs in the galactic halo.

of new features in the antiproton spectrum seems to lurk just behind the currently reachable energies. In fact, with primary fluxes that much enhanced one even has to start worrying about compatibility with the existing low-energy data; such an analysis, however, would be beyond the scope of the present work and warrants a dedicated future study.

Finally, let us address the question whether the next generation of experiments will be able to distinguish between the models that we have presented here. To this end, we consider in Fig. 7 for each model a boost factor that normalizes the maximal deviation from the secondary flux to that of the 1.7 TeV Wino case. For the high energies that we are interested in, the precision of cosmic-ray flux measurements is essentially limited by statistics (see also the remark at the end of Sec. III). For comparison, we have therefore included in Fig. 7 the statistical error after 3 years of data sampling by PAMELA and AMS, respectively, provided that these experiments would measure an antiproton spectrum as induced by LSP annihilations. As we have seen before, a 1.7 TeV LSP can easily be distinguished from the background (even when taking into account the full uncertainty in the spectrum of secondary antiprotons) already by PAMELA. In fact, this is true without having to invoke boost factors at all. In order to discriminate the spectra of the other benchmark DM candidates at a similar confidence level, one has to invoke boost factors from about 150 to 500. While such boost factors may seem rather high from a traditional point of view, we have stressed above that, e.g., in scenarios with DM mini-spikes around IMBHs one would naturally expect even higher values.

When it comes to the actual discrimination between different DM candidates, however, we realize that the prospects are less promising; given the current uncertainty in the secondary flux, as well as the expected statistical errors in the data, neither PAMELA nor AMS will be able to distinguish between different *types* of annihilating WIMPs (i.e. LSP vs LKP). A determination of the WIMP *mass*, on the other hand, will be possible to a certain extent—at least when a clear drop in the spectrum becomes visible (for the DM models considered here this could be the case once the AMS data are available). Note also that there appears in the spectrum a certain degeneracy between the WIMP type and its mass, putting a principle limit on the accuracy of any possible mass determination: for a given mass, the LSP produces an annihilation spectrum that is very similar to that of an LKP, apart from being

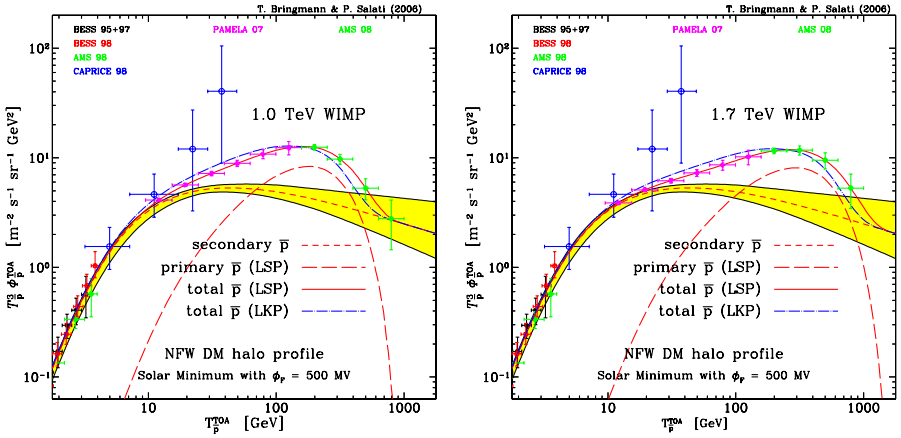

FIG. 7 (color online). The light gray (yellow online) band shows the expected antiproton background for the full range of allowed diffusion parameters. In the left (right) panel, we have added the primary and total fluxes for our 1 TeV (1.7 TeV) benchmark DM models of Table III, assuming an NFW halo profile and a medium set of diffusion parameters; for illustration, and to better compare these models, we have adopted a boost factor of 2 (1050, 330, 270) for the case of an LSP1.7 (LKP1.7, LSP1.0, LKP1.0) dark matter candidate. For the LSP, we also include the expected statistical error after 3 years of data sampling by PAMELA and AMS-02, respectively.

slightly shifted to higher energies. An LKP with a somewhat enhanced mass (by about 10%) would therefore feature a spectrum that is almost indistinguishable from that of the LSP.

V. SUMMARY AND CONCLUSIONS

Upcoming experiments like PAMELA and AMS will extend the upper range of accessible antiproton cosmic-ray energies considerably, from hitherto around 30 GeV to well above 100 GeV. In this article, we have considered the galactic antiproton spectrum at high energies and performed a detailed analysis of what these—and successive—experiments are expected to see. To begin with, we have presented the first discussion of the nontrivial behavior of the antiproton *background* at high energies. Our analysis has been performed in the framework of a two-zone diffusion model, whose parameters can be extracted from the spectra of other cosmic-ray species (the B/C ratio, in particular) in such a way as to give an extremely satisfying explanation of the observed low-energy antiproton data (notice, however, that this is not the conclusion reached in [57] where galactic diffusion is assumed to be anisotropic). We have shown that the diffusion parameters obtained in this way determine, in fact, almost uniquely the spectrum of secondary antiprotons up to energies of around 100 GeV. For larger energies, the uncertainty in the expected spectrum slowly increases, up to a factor of about 6 at 10 TeV. The main reason for this uncertainty lies in the fact that the B/C analysis does not sufficiently constrain the spectral index δ of the diffusion coefficient; this uncertainty will be considerably reduced once experiments like PAMELA and AMS-02 improve the quality and range of existing B/C data. Based on both numerical as well as semianalytical results, we furthermore predict a simple power-law scaling for the high-energy secondary spectrum, above slightly less than 100 GeV, with a spectral index in the range 3.1 to 3.5.

In the second part of this paper, we have investigated the possibility of a contribution from *primary antiprotons* to the high-energy part of the spectrum, originating from the annihilation of DM particles in the galactic halo. To this end, we introduced a set of benchmark models with high DM masses, motivated by DM candidates naturally arising in theories with supersymmetric or extra-dimensional extensions to the standard model of particle physics. We have shown that the expected primary antiproton signal takes in all of these cases a spectral form that is sufficiently different from the background to clearly discriminate it against the latter if the corresponding total fluxes are high enough. For this latter requirement to be satisfied, one usually has to invoke boost factors of $\mathcal{O}(100)$ that at first sight seem rather high (with the interesting exception of a Wino-like DM candidate, see also [21]). As a side result of the present work, however, we have also derived the expected boost factors in the IMBH scenario of [46] and demonstrated that in this case, in fact, they are even higher than what is needed for a clear attribution of the observed signal to a DM (as opposed to secondary antiproton) origin. We, furthermore, note that the most recent, high-resolution simulations of gravitational clustering [58] hint at a considerable DM fraction to be distributed in clumps of highly enhanced DM densities, which potentially would lead to large boost factors, too.

When it comes to the possibility of distinguishing between different DM candidates, however, the antiproton spectrum does not turn out to be very well suited and other indirect DM detection methods (gamma rays, in particular) are probably more promising in that respect. The mass of the annihilating DM particle, on the other hand, may

eventually be determined, to a fair accuracy, from the antiproton spectrum alone; a comparison with the result of other DM searches would then give an important, independent piece of information. It is also worthwhile to study in this context the cross correlation of antiproton signals with DM-induced features in the spectrum of other charged cosmic-ray species (for the LKP, e.g., this would be a pronounced peak in the *positron* spectrum that necessarily has to appear if the antiproton spectrum shows an LKP-induced distortion [20,59]—a feature that is not shared by LSP DM candidates).

To conclude, measurements of the galactic antiproton spectrum are an important test bed for our understanding of the propagation of charged particles through the galaxy and the diffusive structure of the Milky Way halo. As a means of indirect DM detection, antiprotons are probably not the single-most promising species; we would like to stress, however, that one should, rather, focus on the complementarity of different approaches, to which antiproton measurements would then have the potential of providing an important contribution.

ACKNOWLEDGMENTS

It is a pleasure to thank Pierre Brun for many interesting discussions on antiproton fragmentation functions in the early stages of this work. We are, furthermore, grateful to Laurent Derôme who helped us with the antiproton differential production cross section in $p + A$ interactions and to Joakim Edsjö for support with the DARKSUSY package. P. S. would like to thank the French programme national de cosmologie PNC for its financial support. T. B. warmly acknowledges the hospitality and pleasant atmosphere of the Laboratoire d'Annecy-le-Vieux de Physique Théorique (LAPTH), where part of this work was performed.

[1] S. Orito *et al.* (BESS Collaboration), Phys. Rev. Lett. **84**, 1078 (2000).
[2] T. Maeno *et al.* (BESS Collaboration), Astropart. Phys. **16**, 121 (2001).
[3] M. Boezio *et al.* (WiZard/CAPRICE Collaboration), Astrophys. J. **561**, 787 (2001).
[4] M. Aguilar *et al.* (AMS Collaboration), Phys. Rep. **366**, 331 (2002); **380**, 97(E) (2003).
[5] F. Donato, D. Maurin, P. Salati, R. Taillet, A. Barrau, and G. Boudoul, Astrophys. J. **563**, 172 (2001).
[6] D. Maurin, F. Donato, R. Taillet, and P. Salati, Astrophys. J. **555**, 585 (2001).
[7] P. Picozza *et al.*, astro-ph/0608697; http://wizard.roma2.infn.it/pamela/.
[8] F. Barao (AMS-02 Collaboration), Nucl. Instrum. Methods Phys. Res., Sect. A **535**, 134 (2004); http://ams.cern.ch/AMS/.
[9] D. N. Spergel *et al.*, astro-ph/0603449.
[10] G. Jungman, M. Kamionkowski, and K. Griest, Phys. Rep. **267**, 195 (1996); L. Bergström, Rep. Prog. Phys. **63**, 793 (2000); G. Bertone, D. Hooper, and J. Silk, Phys. Rep. **405**, 279 (2005).
[11] J. Silk and M. Srednicki, Phys. Rev. Lett. **53**, 624 (1984).
[12] A. Buffington, S. M. Schindler, and C. R. Pennypacker, Astrophys. J. **248**, 1179 (1981).
[13] L. Bergström, J. Edsjö, and P. Ullio, Astrophys. J. **526**, 215 (1999).
[14] T. Appelquist, H. C. Cheng, and B. A. Dobrescu, Phys. Rev. D **64**, 035002 (2001).
[15] H. C. Cheng, K. T. Matchev, and M. Schmaltz, Phys. Rev. D **66**, 036005 (2002); G. Servant and T. M. P. Tait, Nucl. Phys. **B650**, 391 (2003).
[16] See, e.g., H. Baer, T. Krupovnickas, S. Profumo, and P. Ullio, J. High Energy Phys. 10 (2005) 020; U. Chattopadhyay, D. Choudhury, M. Drees, P. Konar, and D. P. Roy, Phys. Lett. B **632**, 114 (2006), and references therein.
[17] J. Hisano, S. Matsumoto, and M. M. Nojiri, Phys. Rev. Lett. **92**, 031303 (2004); J. Hisano, S. Matsumoto, M. M. Nojiri, and O. Saito, Phys. Rev. D **71**, 063528 (2005).
[18] P. Ullio, astro-ph/9904086.
[19] A. M. Lionetto, A. Morselli, and V. Zdravkovic, J. Cosmol. Astropart. Phys. 09 (2005) 010.
[20] T. Bringmann, J. Cosmol. Astropart. Phys. 08 (2005) 006.
[21] J. Hisano, S. Matsumoto, O. Saito, and M. Senami, Phys. Rev. D **73**, 055004 (2006).
[22] L. C. Tan and L. K. Ng, Phys. Rev. D **26**, 1179 (1982).
[23] L. C. Tan and L. K. Ng, J. Phys. G **9**, 227 (1983).
[24] J. Lavalle, J. Pochon, P. Salati, and R. Taillet, Astron. Astrophys. **462**, 827 (2007).
[25] D. Maurin, R. Taillet, and C. Combet, astro-ph/0609522.
[26] R. P. Duperray, C.-Y. Huang, K. V. Protasov, and M. Buénerd, Phys. Rev. D **68**, 094017 (2003).
[27] J. R. Letaw *et al.*, Astrophys. J. Suppl. Ser. **51**, 271 (1983).
[28] J. Engel, T. K. Gaisser, P. Lipari, and T. Stanev, Phys. Rev. D **46**, 5013 (1992).
[29] See, e.g., J. S. Perko, Astron. Astrophys. **184**, 119 (1987).
[30] T. Sanuki *et al.*, Astrophys. J. **545**, 1135 (2000).
[31] J. Alcaraz *et al.* (AMS Collaboration), Phys. Lett. B **472**, 215 (2000); J. Alcaraz *et al.* (AMS Collaboration), Phys. Lett. B **490**, 27 (2000); **494**, 193 (2000).
[32] A. M. Lionetto, A. Morselli, and V. Zdravkovic, J. Cosmol. Astropart. Phys. 09 (2005) 010.
[33] A. W. Strong and I. V. Moskalenko, Astrophys. J. **509**, 212 (1998).
[34] T. Sjöstrand, P. Eden, C. Friberg, L. Lonnblad, G. Miu, S. Mrenna, and E. Norrbin, Comput. Phys. Commun. **135**, 238 (2001).

[35] P. Gondolo, J. Edsjö, P. Ullio, L. Bergström, M. Schelke, and E. A. Baltz, J. Cosmol. Astropart. Phys. 07 (2004) 008.
[36] J. F. Navarro, C. S. Frenk, and S. D. M. White, Astrophys. J. **490**, 493 (1997).
[37] B. Moore, S. Ghigna, F. Governato, G. Lake, T. Quinn, J. Stadel, and P. Tozzi, Astrophys. J. **524**, L19 (1999).
[38] J. Diemand, B. Moore, and J. Stadel, Mon. Not. R. Astron. Soc. **353**, 624 (2004).
[39] V. R. Eke, J. F. Navarro, and M. Steinmetz, Astrophys. J. **554**, 114 (2001).
[40] N. Fornengo, L. Pieri, and S. Scopel, Phys. Rev. D **70**, 103529 (2004).
[41] V. S. Berezinsky, A. V. Gurevich, and K. P. Zybin, Phys. Lett. B **294**, 221 (1992).
[42] A. Barrau, P. Salati, G. Servant, F. Donato, J. Grain, D. Maurin, and R. Taillet, Phys. Rev. D **72**, 063507 (2005).
[43] T. Bringmann, Ph.D thesis, Stockholm University, 2005.
[44] A. M. Green, S. Hofmann, and D. J. Schwarz, J. Cosmol. Astropart. Phys. 08 (2005) 003.
[45] J. Diemand, B. Moore, and J. Stadel, Nature (London) **433**, 389 (2005).
[46] G. Bertone, A. R. Zentner, and J. Silk, Phys. Rev. D **72**, 103517 (2005).
[47] P. Brun, G. Bertone, J. Lavalle, P. Salati, and R. Taillet, arXiv:0704.2543.
[48] S. Profumo and C. E. Yaguna, Phys. Rev. D **70**, 095004 (2004).
[49] P. Ullio, J. High Energy Phys. 06 (2001) 053.
[50] J. Hisano, S. Matsumoto, M. Nagai, O. Saito, and M. Senami, hep-ph/0610249.
[51] L. Bergström, T. Bringmann, M. Eriksson, and M. Gustafsson, Phys. Rev. Lett. **95**, 241301 (2005).
[52] U. Chattopadhyay, D. Das, P. Konar, and D. P. Roy, hep-ph/0610077.
[53] M. Kakizaki, S. Matsumoto, and M. Senami, Phys. Rev. D **74**, 023504 (2006).
[54] K. Kong and K. T. Matchev, J. High Energy Phys. 01 (2006) 038.
[55] S. Profumo, Phys. Rev. D **72**, 103521 (2005).
[56] F. Donato, N. Fornengo, D. Maurin, and P. Salati, Phys. Rev. D **69**, 063501 (2004).
[57] W. de Boer, I. Gebauer, C. Sander, M. Weber, and V. Zhukov, astro-ph/0612462.
[58] J. Diemand, M. Kuhlen, and P. Madau, Astrophys. J. **657**, 262 (2007).
[59] D. Hooper and G. D. Kribs, Phys. Rev. D **70**, 115004 (2004).